Amorphous phase formation of the pseudo-binary Al_2O_3–ZrO_2 alloy during plasma spray processing

H.-J. KIM
Research Institute of Industrial Science and Technology, Pohang, 790-600, Korea

Y. J. KIM
Center for Advanced Aerospace Materials, Pohang University of Science and Technology, Pohang, 790-784, Korea

Thick deposits of the Al_2O_3–ZrO_2 with near eutectic compositions were prepared by plasma-spray deposition and subjected to heat treatment to investigate the crystallization and phase transformation behaviors. The structures of as-sprayed deposits are mostly amorphous and a small amount of t-ZrO_2 and γ-Al_2O_3 particles with a diameter of approximately 20 nm are also present. Simultaneous crystallization of t-ZrO_2 and γ-Al_2O_3 from the glass occurs at 945 °C, followed by δ- and α-Al_2O_3 above 1000 °C, and only α-Al_2O_3 are observed above 1200 °C. Phase transformation of t-ZrO_2 to m-ZrO_2 occurs at 1213 °C. There is no appreciable difference in amorphous formation and subsequent crystallization and phase transformation behaviors with two different feedstock powder sizes. It is shown that it is feasible to produce the thick amorphous Al_2O_3–ZrO_2 materials with proper control of plasma spraying process parameters.

1. Introduction

Plasma spray deposition processing offers perhaps the highest potential for the microstructural control benefits of high temperature materials achieved by rapid solidification processing. Throughout the analysis of rapid solidification processing, the conditions of nucleation and liquid undercooling behavior have been recognized for the strong influence that they can exert on the initial stage of solidification structure formation [1]. Moreover, the amount of undercooling (ΔT) prior to and during solidification has the most pronounced effect on the nucleation of equilibrium and nonequilibrium crystalline phases as well as on amorphous phases. Thus, it is realized as being a central factor in determining microstructural development by controlling phase selection during solidification. The phase selection range includes various novel metastable phases in addition to the distinct refinement of scale in the final microstructure products, resulting from rapid crystallization kinetics and, ultimately, amorphous phase formation with the proper amount of undercooling down to the glass transition temperature, Tg, as well.

Al_2O_3–ZrO_2 system has been extensively investigated because Al_2O_3 with dispersed tetragonal ZrO_2 was found to have transformation toughness bearing a wide variety of applications [2–4]. It is well established that pure zirconia has three polymorphic, fluorite-based, equilibrium structures [5]:

$$\text{liquid} \overset{\sim 2680\,^\circ\text{C}}{\leftrightarrow} \text{cubic (c)} \overset{\sim 2370\,^\circ\text{C}}{\leftrightarrow} \text{tetragonal (t)} \overset{950 \sim 1150\,^\circ\text{C}}{\leftrightarrow} \text{monoclinic (m)}$$

It is known that the transformation toughness is based on the martensitic transformation of t-ZrO_2 to m-ZrO_2. The role of Al_2O_3 for the stabilization of tetragonal ZrO_2 is controversial. Kagawa et al. [6] reported that the amount of the m-ZrO_2 decreased with the increase in Al_2O_3 content, thus indicating the stabilization of the t-ZrO_2 by the Al_2O_3. However, McKittrick *et al.* [7] suggested that Al_2O_3 did not chemically stabilize the t-ZrO_2 crystal structure because monoclinic and tetragonal particles of similar size showed no difference in Al_2O_3 concentration.

Several studies have reported amorphous materials of the Al_2O_3–ZrO_2 eutectic composition (42 wt % or 37 mol % ZrO_2) obtained through plasma spraying [8], laser-splatting [8], electrohydrodynamic atomization [9], and melt extraction [7, 10]. With all of these methods, the glassy materials did not comprise the bulk of the solidified product and were found only in small samples or in small areas of a sample. For example, it was found that the amorphous state is accessible between 0 and 75 wt % ZrO_2 with a peak of about 1 μm in the maximum size of amorphous powders at the eutectic composition of Al_2O_3-42 wt % ZrO_2 [9] because the eutectic composition has the lower melting temperature and greater potential for obtaining amorphous structures.

This article reports on the amorphous formation of rather thick (over 2 mm in thickness) Al_2O_3–ZrO_2 deposits by plasma spray deposition. The structures and crystallization behaviors of as-sprayed and subsequent heated treated deposits with near eutectic compositions are assessed using SEM, TEM, DTA, and XRD experimental techniques.

TABLE I Properties of feedstock powders used in this study

Specimen code	Chemical composition (wt %)	Size range (μm)	Manufacturing method	Phases[a]
	Al_2O_3 57.9			t-ZrO_2 (64%)
A (Fine)	ZrO_2 39.8	5-23	Fused	α-Al_2O_3
	TiO_2 2.3			m-ZrO_2 (36%)
	Al_2O_3 59.1			m-ZrO_2 (88%)
B (Coarse)	ZrO_2 38.8	22-45	Agglomerated	α-Al_2O_3
	TiO_2 2.1		& sinterd	t-ZrO_2 (12%)

[a]Measured by X-ray diffraction according to Ref. [11].

TABLE II Plasma-spraying parameters

Parameters	A	B
Primary gas, Ar (SLPM)	40	40
Secondary gas, H_2 (SLPM)	14	14
Voltage (V)	73	72
Current (A)	550	600
Spray distance (mm)	120	120
Spray rate (g/min)	30	30

2. Experimental procedure

Table I summarizes the characteristics of the feedstock powders investigated. A small addition of TiO_2 is probably to stabilize the tetragonal phase of ZrO_2. The compositions of both powders (A and B) are near eutectic composition, but the size of A powder is finer than that of B powder. It is interesting to note that the main phase of finer (A) powder is the tetragonal ZrO_2, but the main phase of coarser (B) powder is the monoclinic ZrO_2. The deposits were prepared by conventional plasma spraying with a Metco-Sulzer F4 gun (PT-M1100). The plasma-spray parameters are given in Table II. The deposits were sprayed onto low carbon steel with 5 mm thickness and then the substrate was dissolved using a chemical etch. Samples were ultrasonically cleaned and dried before each measurement.

The porosity of the as-sprayed thick deposits was determined with a mercury intrusion porosimeter (maximum pressure, 60,000 psi corresponding to pore size range of 0.003 to 300 μm). The phase compositions of the deposits were measured in the as-sprayed and heat-treated state using X-ray diffraction with CuKα radiation. DTA was used to identify the crystallization and any phase transformation temperatures. The samples were heated at 10 °C/min between 25–1300 °C using an Al_2O_3 powder reference standard.

For the TEM study, as-sprayed thick deposits were cut to about 0.8 mm thickness with a diamond saw and mechanically polished down to about 100 μm and then ion-beam thinned, followed by deposition of a thin layer of carbon before examination under a Philips CM200 operated at 200 kV.

The heat treatment of the as-sprayed deposits were carried out for one hour in vacuum at 900–1300 °C. The vacuum was maintained with 2×10^{-5} torr during the whole heat treatment cycle.

3. Results and discussion

Table III summarizes the characteristics of the plasma sprayed thin and thick deposits investigated. Porosity values of thick deposits are a little lower than that (around 10%) of expected probably because a mercury intrusion porosimeter can measure only the open pores, excluding closed pores. Fig. 1 shows the back scattered electron image of the cross section of plasma-sprayed thick deposit using coarser (B) powders. It shows a typical of the plasma-sprayed ceramic coatings, that is, there are numerous pores, crack, and unmelted particles. It was determined by EDS that bright lamella are ZrO_2-rich and dark lamella are Al_2O_3-rich. The structure of the thermal sprayed deposits is inhomogeneous and composed of lamella that may have different chemical compositions.

Fig. 2 shows the X-ray diffraction pattern of the Al_2O_3–ZrO_2 thick deposit surface. The X-ray

TABLE III Characteristics of as-sprayed deposits

Specimen description		Thickness (mm)	Porosity (%)	Hardness (HV)	Bond strength (kg/cm^2)
A	Thin	0.15	10.1[a]	513 (444-547)[c]	541
	Thick	2.10	5.9[b]	460 (435-483)[d]	—
B	Thin	0.16	9.1[a]	594 (512-666)[c]	478
	Thick	2.15	4.3[b]	493 (434-541)[a]	—

[a]Measured by image analysis. [b]Measured by MIP (Mercury Intrusion Porosimeter). [c]Measured by 300 gram load at cross section. [d]Measured by 5 kg load at cross section.

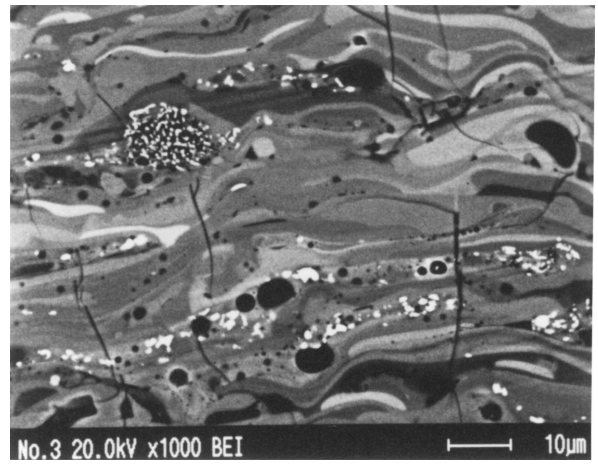

Figure 1 Back scattered electron image of the cross section of the plasma-sprayed ZrO_2–Al_2O_3 thick deposit.

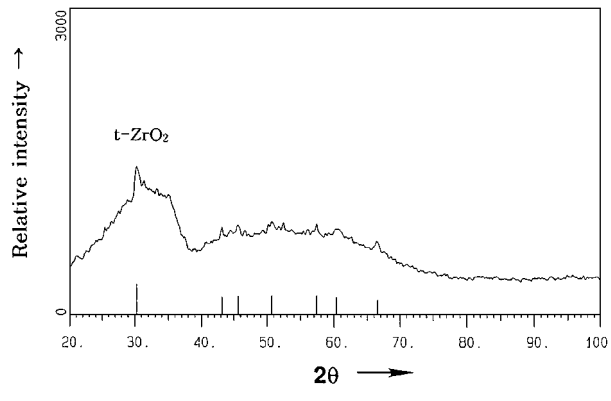

Figure 2 X-ray diffraction pattern of the plasma-sprayed Al_2O_3–ZrO_2 thick deposit surface. All of the as-sprayed deposits show identical diffraction patterns.

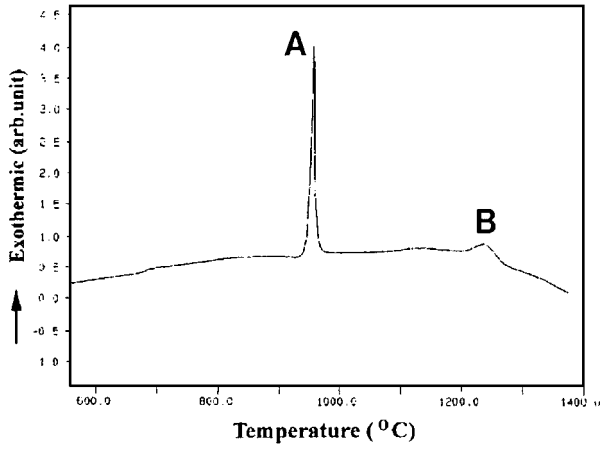

Figure 3 DTA result for plasma-sprayed Al_2O_3–ZrO_2 thick deposit.

diffraction pattern suggests that the structures of as-sprayed deposits are mostly amorphous, and trace of tetragonal ZrO_2 crystals are present. It should be noted that tetragonal ZrO_2 phase formed during the plasma-spray processing is called "nontransformable tetragonal" that can be transformed to monoclinic phase only with heat treatment [11, 12]. It is differentiate with transformable tetragonal phase that can be transformed to monoclinic phase when stressed. Further discussion will focus on only the thick deposits because X-ray diffraction patterns are almost identical to all of the as-sprayed samples investigated.

Fig. 3 shows the DTA curve of thick deposit sample with a thickness of over 2 mm measured at a heating rate of 10 °C/min. The amorphous phase transforms to crystalline phases accompanied by a sharp exothermic reaction (A peak in the figure) with the onset temperature of about 946 °C. There is no appreciable difference in the crystallization temperature (945–946 °C), the exothermic peak temperature (956–957 °C), and the exothermic reaction behavior (ΔH) with two thick samples. The DTA curve also shows a broad exothermic peak (B peak in the figure) above 1200 °C. The onset and peak temperatures of the broad peak are 1213 and 1238 °C, respectively.

Fig. 4 shows a transmission electron micrograph and selected area diffraction patterns of as-sprayed Al_2O_3–ZrO_2 thick deposit. Most of regions are amorphous in TEM examinations as expected from X-ray diffraction patterns. No long range order was noted in the amorphous areas as indicated by the halos of the selected area diffraction pattern (Region A in Fig. 4). However, the amorphous regions occasionally contained fine crystallites having a size of around 20 nm (Region B in Fig. 4). Table IV lists the result of the indexing of the diffraction pattern of region B, and shows that the particles are likely to be the mixtures of tetragonal ZrO_2 and γ-Al_2O_3. Results of chemical analysis by EDS in the TEM showed that darker regions are ZrO_2-rich and lighter regions are Al_2O_3-rich. The hypothetical free energy functions suggest that there is a range of compositions in the vicinity of the eutectic where crystallization to a single phase is thermodynamically forbidden [13]. It was also reported that the lamellar structure of the eutectic in the melt-extracted Al_2O_3-42 wt % ZrO_2 alloy became increasingly finer with increasing cooling rate, and at the highest cooling rates was replaced by a fully amorphous structure [10]. However, the lamellar structure of the eutectic in our plasma-sprayed samples was not observed.

TABLE IV Indexing of SAD pattern of Fig. 4

	t-ZrO_2		γ-Al_2O_3	
d_{obs}	d	hkl	d	hkl
3.04	2.995	$10\bar{1}$	—	—
2.51	2.574	110	—	—
2.23	—	—	2.28	222
2.01	—	—	1.977	400
1.86	1.841	112	—	—
1.57	1.555	211	—	—

Fig. 5 shows the X-ray diffraction patterns of heat-treated samples of the plasma-sprayed thick deposits. Based on the results of XRD and DTA, it is assumed that simultaneous crystallization of t-ZrO_2 and γ-Al_2O_3 occurs at 945–946 °C corresponding a sharp exothermic peak in the DTA curve. A broad exothermic peak above 1200 °C is associated with the phase transformation of t-ZrO_2 to m-ZrO_2. It is worth while to note that α-Al_2O_3 and δ-Al_2O_3 peaks appear and replace γ-Al_2O_3 at 1100 °C and only α-Al_2O_3 peaks are observed above 1200 °C. This result conforms to previous observations that thermal-sprayed metastable γ-Al_2O_3 is transformed to δ- and α-Al_2O_3 above 880 and 1000 °C, respectively [14, 15]. A summary of the X-ray diffraction results is listed in Table V.

Investigators have reported the crystallization of metastable phases with highly extended solid solubilities in the ZrO_2–Al_2O_3 system [8–10, 16]. They noted systematic increases in crystallization temperature with Al_2O_3 content [13, 16]. The crystallization temperature reached maximum (about 980 °C) at around eutectic composition. For example, simultaneous crystallization of γ-Al_2O_3 and t-ZrO_2 occurs at 870-980 °C and the γ-Al_2O_3 transforms to α-Al_2O_3 at 1160–1220 °C for amorphous Al_2O_3–ZrO_2 composite powders with 5–30 mol % ZrO_2 [17]. However, other papers reported that the first phase to crystallize from the glass was t-ZrO_2 at 944 °C, followed by δ-Al_2O_3 above 1000 °C, α-Al_2O_3 and m-ZrO_2 appeared at 1450 °C for melt-extracted Al_2O_3–ZrO_2 eutectic composition [7, 10]. This discrepancy is probably attributed to the difference in amorphous amount of the materials. This leaves further investigations.

In the plasma spray deposition associated with rapid solidification processes, it is important to consider that two distinct but closely related processing conditions prevail. The first condition involves a containerless

TABLE V Summary X-ray diffraction results

Temperature (°C)	Phases
900	t-ZrO_2 only
1000	t-ZrO_2 with γ-Al_2O_3
1100	t-ZrO_2 with δ-Al_2O_3, α-Al_2O_3
1200	t-ZrO_2 with α-Al_2O_3, m-ZrO_2
1300	m-ZrO_2 with t-ZrO_2, α-Al_2O_3

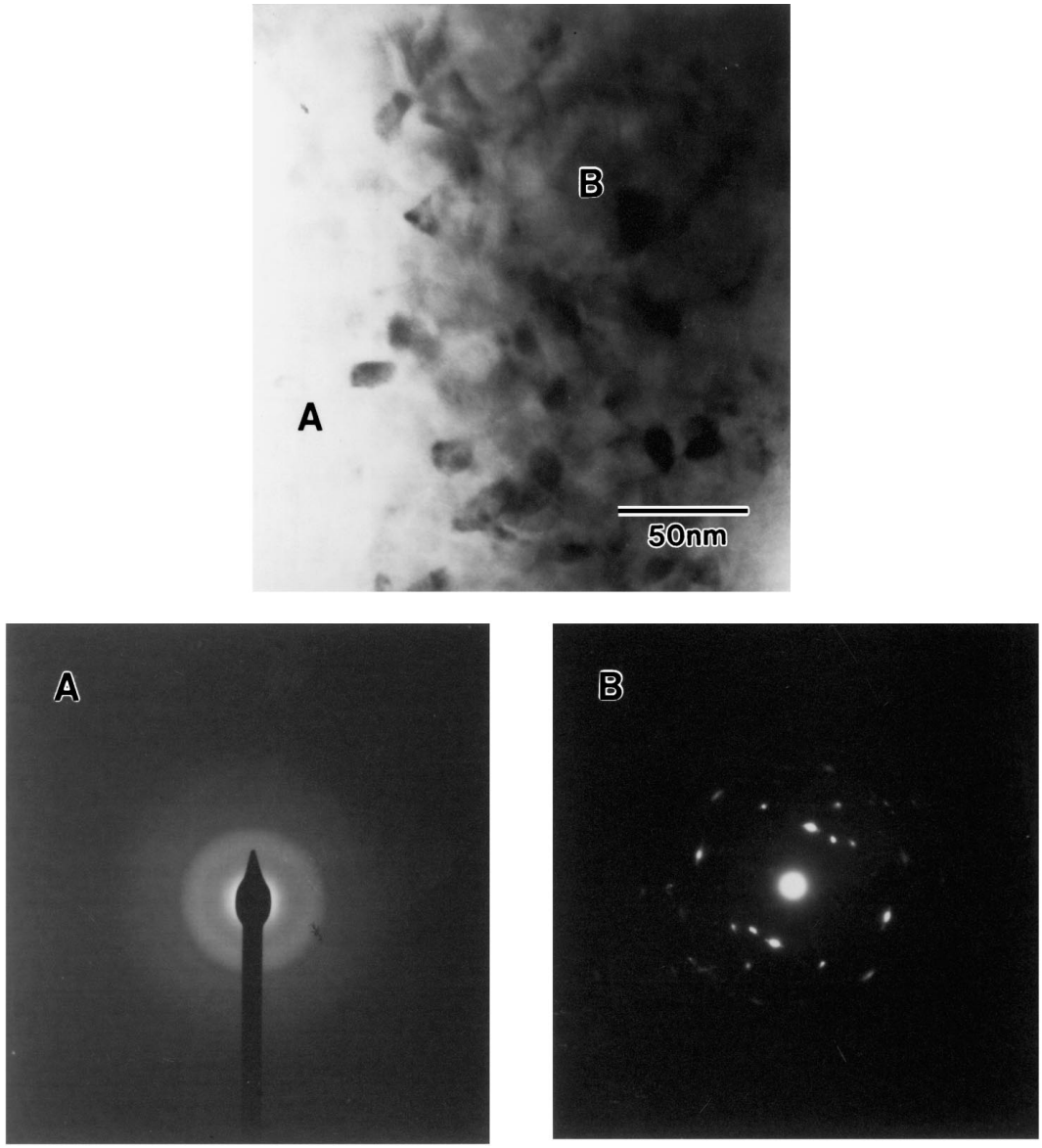

Figure 4 Transmission electron micrograph and selected area diffraction patterns of plasma-sprayed Al_2O_3–ZrO_2 deposit showing amorphous structure (region A) and fine crystallites (region B). Zone directions of t-ZrO_2 and γ-Al_2O_3 are $[1\,\bar{3}\,1]$ and $[0\,\bar{1}\,1]$, respectively.

processing aspect in the liquid droplets during flight prior to impact on the deposition surface. The containerless processing represents a technique combining rapid cooling rate of rapid solidification aspect with slow cooling rate of controlled undercooling by elimination of possible heterogeneous nucleation sites from the container wall. Examples include containerless drop tube processing allowing for significant levels of liquid undercooling through control of processing parameters, such as sample size, surface coating, and cooling rate [18, 19]. In the second, a dynamic processing condition is dominated at the moment of impact on the substrate. In this case, the optimum processing condition of droplets for deposition upon impact is the mixture of liquid and solid within the droplets [20] resulting from the previous processing condition (i.e., during the flight of liquid droplets). These closely related processing stages indicate that the most fundamental and key factor in determining the microstructural evolution during entire deposition process is the degree of droplet solidification at the point of deposition.

For plasma spraying, the cooling rates are reported to be the order of 10^6 K/sec by calculating heat transfer between a plasma-sprayed droplet and a highly conducting metal surface [21, 22]. Thus, the formation of glass depends on the competition between the cooling rate in the liquid and the highest nucleation rate among all the thermodynamically feasible crystalline phases.

Fine particles are thought to solidify at higher rates than larger diameter particles [9, 23, 24]. For example, fine particles yield greater proportions of metastable gamma phase than do large particles for the plasma-spraying of Al_2O_3 [25]. However, this phenomenon can be overcome by optimizing the torch parameters [26]. In our samples, two different feedstock powder sizes do not show any appreciable differences in amorphous formation and subsequent crystallization behaviors from XRD, DTA, and TEM investigations. Therefore, it is feasible to produce the bulk amorphous Al_2O_3–ZrO_2 materials with proper control of plasma spraying process parameters.

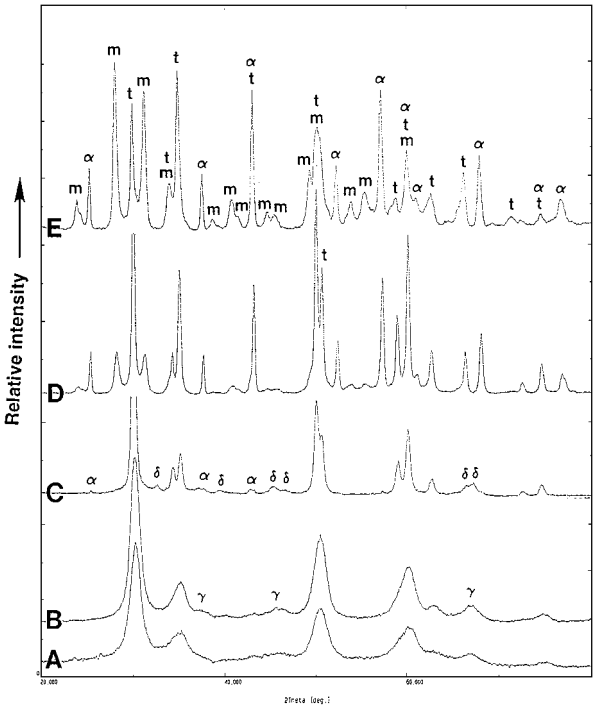

Figure 5 X-ray diffraction patterns of heat-treated Al_2O_3–ZrO_2 deposits produced by plasma-spraying. (t: tetragonal-ZrO_2, m: monoclinic-ZrO_2, γ: γ-Al_2O_3, α: α-Al_2O_3, δ: δ-Al_2O_3) (A) 900 °C (B) 1000 °C (C) 1100 °C (D) 1200 °C (E) 1300 °C.

4. Conclusions

Thin (0.15 mm in thickness) and thick deposits (over 2 mm in thickness) of the Al_2O_3–ZrO_2 with near eutectic compositions were successfully prepared by plasma-spray deposition and subjected to heat treatment in vacuum to investigate the crystallization and phase transformation behaviors. The structures of as-sprayed deposits are mostly amorphous and small amount of t-ZrO_2 and γ-Al_2O_3 particles with a diameter of approximately 20 nm are also present. Simultaneous crystallization of t-ZrO_2 and γ-Al_2O_3 from the glass occurs at 945 °C, followed by δ- and α-Al_2O_3 above 1000 °C, and only α-Al_2O_3 are observed above 1200 °C. Phase transformation of t-ZrO_2 to m-ZrO_2 occurs at 1213 °C. There is no appreciable difference in amorphous formation and subsequent crystallization and phase transformation behaviors with two different feedstock powder sizes. It is shown that it is feasible to produce the bulk amorphous Al_2O_3–ZrO_2 materials with proper control of plasma spraying process parameters.

References

1. J. H. PEREPEZKO, *Mater. Sci. Eng.* **65** (1984) 125.
2. J. E. PATCHETT, *Key Engineering Materials* **122**–**124** (1996) 325.
3. A. PETITBON, D. GUIGNOT, U. FISCHER and J. M. GUILLEMOT, *Mater. Sci. Eng.* **A121** (1989) 545.
4. A. PETITBON, L. BOQUET, and D. DELSART, *Surf. Coat. Technol.* **49** (1991) 57.
5. M. RUHLE and A. H. HEUER, "Phase transformations in ZrO_2-containing ceramics: The martensitic reaction in t-ZrO_2," *Advances in Ceramics*, Vol. 12, *Science and Technology of Zirconia II*, edited by N. Claussen, M. Ruhle and A. H. Heuer, (American Ceramic Society, Columbus, OH, USA, 1984) pp. 14–31.
6. M. KAGAWA, M. KIKUCHI, Y. SYONO and T. NAGAE, *J. Am. Ceram. Soc.* **66** (1983) 751.
7. J. McKITTRICK, G. KALONJI and T. ANDO, *J. Non-Cryst. Sol.* **94** (1987) 163.
8. G. KALONJI, J. MCKITTRICK, and L. W. HOBBS, "Application of rapid solidification theory and practice to Al_2O_3-ZrO_2 ceramics," *Advances in Ceramics*, Vol. 12, *Science and Technology of Zirconia II*, edited by N. Claussen, M. Ruhle, and A. H. Heuer, (American Ceramic Society, Columbus, OH, USA, 1984) pp. 816–825.
9. V. JAYARAM, T. WHITNEY, C. G. LEVI, and R. MEHRABIAN, *Mater. Sci. Eng.* **A124** (1990) 65.
10. T. ANDO and Y. SHIOHARA, *J. Am. Ceram. Soc.* **74** (1991) 410.
11. R. A. MILLER, J. L. SMIALEK and R. G. GARLICK, *Advances in Ceramics*, Vol. 3, *Science and Technology of Zirconia II*, edited by A. H. Heuer and L. W. Hobbs (American Ceramic Society, Columbus, OH, USA, 1982) pp. 241–253.
12. J. R. BRANDON and R. TAYLOR, *Surf. Coat. Technol.* **46** (1991) 75.
13. M. L. BALMER, F. F. LANGE and C. G. LEVI, *J. Am. Ceram.* Soc. **77** (1994) 2069.
14. R. MCPHERSON, *J. of Mater. Sci.* **15** (1980) 3141.
15. L. PAWLOWSKI, *Surf. Coat. Technol.* **31** (1987) 103.
16. O. YAMAGUCHI, M. SHIRAI and M. YOSHINAKA, *J. Am. Ceram. Soc.* **71** (1988) C 510.
17. Y. MATSUMOTO, K. HIROTA, O. YAMAGUCHI, S. INAMURA, H. MIYAMOTO, N. SHIOKAWA and K. TSUJI, *ibid.* **76** (1993) 2677.
18. A. J. DREHMAN and D. TURNBULL, *Scripta Metall.* **15** (1981), 543.
19. R. F. COOPER, W. Y. YOON and J. H. PEREPEZKO, *J. Am. Ceram. Soc.* **74** (1991) 1312.
20. B. P. BEWLAY and B. CANTOR, *Metall. Trans.* **21B** (1990) 899.
21. M. MOSS, *Acta Metall.* **16** (1968) 321.
22. S. SAFAI and H. HERMAN, *Treatise Mater. Sci. Technol.* **20** (1981) 183.
23. Y. KAWAMURA, H. KATO, A. INOUE and T. MASUMOTO, *International J. of Powder Metallurgy* **33** (1997) 50.
24. A. INOUE, T. MASUMOTO, T. EKIMOTO, S. FURUKAWA, Y. KURODA and H. S. CHEN, *Metall. Trans. A* **19A** (1988) 235.
25. H. G. WANG, Y. M. ZHU and H. HERMAN, *J. of Mater. Sci.* **24** (1989) 4414.
26. G. N. HEINTZE and S. UEMATSU, *Surf. Coating Technol.* **50** (1992) 213.

Received 26 July
and accepted 26 August 1998